Too hot to handle? Synchrotron X-ray damage of lipid membranes and mesophases†

Vadim Cherezov, Ken M. Riedl and Martin Caffrey*

Biochemistry, Biophysics, Chemistry, The Ohio State University, 100 West 18th Avenue, Columbus, OH 43210, USA. E-mail: caffrey.1@osu.edu

The call for brighter synchrotron X-radiation sources for use in structural biology research is barely audible as we enter the new millennium. Our brightest sources are already creating havoc when used at design specifications because of radiation damage. The time is long overdue to take stock of where we are and where we wish to go with regards to using existing sources and to designing new ones. The problem of radiation damage is particularly acute in studies involving kinetics and mechanisms where cryo-techniques are not always viable. Accordingly, we need to understand the very nature of radiation damage and to devise means of minimizing it. This is the thrust of the current report as applied to lipid membranes and mesophases. The experiments were performed at the most brilliant beamlines at CHESS, the APS and the ESRF. Two very different types of radiation damage are reported here. One involves a dramatic phase transformation and the other a disordering of lamellar stacking. How beam energy and dose rate affect damage is also discussed. The work highlights the free-radical-mediated nature of the damage process and the need for additional studies if the most efficient use is to be made of an important resource, synchrotron radiation.

Keywords: aging; cubic phase; energy effects; free radicals; heating; hexagonal phase; inverse dose-rate; lamellar phase; phase transitions.
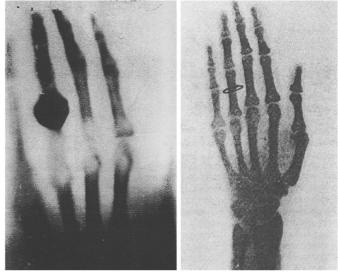
1. Introduction

In these introductory remarks, we attempt to put our contribution to this workshop on radiation damage in a historical context. Thus, a more apt title for the report might be 'Blame it on the Ring' or 'The Curse of the Ring'. The workshop was conducted at the site of a very special type of ring, one that produces a torrent of X-rays that can at times be 'too hot to handle'. But our problems harken back to a very different kind of ring: the one shown in Fig. 1(a). Röntgen produced this impressive image of his wife's hand, where a ring figures prominently on her finger, with the first synthetic X-rays in 1895. The exposure time was 15 min. Within four months, a company published an advertisement (Fig. 1b) claiming to have available an instrument that could produce a vastly improved image of a hand, complete with ring, in a mere 3 min, corresponding to a reduction in exposure time of a factor of five. Thus, the race was on back in the late 1800s to produce 'bigger and better' X-ray machines. The race continues today and is in part responsible for this workshop, which was organized to address issues that have arisen because of what amounts to 'too much of a good thing'.

In what follows, we recount our experiences with radiation damage using synchrotron radiation. The biomaterials we have worked with

most intensively in this context are lipids, one of the major components of biological membranes. We begin by providing some background on membranes and lipids and the liquid-crystal phases that lipids form. We are interested in physiological processes that involve membranes and have chosen to use X-rays for structure elucidation. In this work, particular attention is paid to the dynamic features of biological membranes. As a result, we have resorted to synchrotron sources because the prodigious photon flux they provide facilitates the necessary time-resolved measurements. This is where our problems with radiation damage began.

1.1. Lipids and biomembranes

Fig. 2(a) shows a thin section of a rat liver cell where the darkly staining lines highlight the biomembrane. This figure suggests that membranes figure prominently in the life of the cell. The cell membrane can be viewed as a bimolecular lipid leaflet, in and on which are situated a variety of proteins and other molecules (Fig. 2b). In our work, we take a holistic view of the membrane, and study both the lipid and protein components. However, in this presentation, the lipid component alone will be addressed. A representative glycero-phospholipid is shown in Fig. 2(c). Lipids are amphiphiles, with a polar and an apolar part built into the same molecule.

Lipids are interesting for several reasons. As illustrated in Fig. 2(d), they have the capacity to spontaneously self-assemble. With apologies to Hokusai, this woodprint has been modified to illustrate the process of self-assembly. Thus, at the air–water interface is a monomolecular lipid film. Elsewhere, we see a bilayered vesicle and micelles. Spontaneous self-assembly does not require a genetic blueprint nor indeed an energy input in the form of adenosine triphosphate. It is a spontaneous process that has its origins in the hydrophobic effect. The latter in turn depends on what might be referred to as the narcissistic properties of water, the fact that water

Figure 1
The race to produce bigger and better X-ray devices began with the publication of these X-ray images in 1895. (a) Image of 'Hand Mit Ringen' taken 22 December 1895. Photograph courtesy of Otto Glasser, *Wilhelm Conrad Rontgen und die Geschichte der Rontgenstrahlen*, 1931, Springer-Verlag, Berlin. (b) Advertisement for images attainable using a Thomson Universal Tube produced by Edison Decorative and Miniature Lamp Department, Harrison, NJ, as published in *Electrical Engineer* four months after (a).
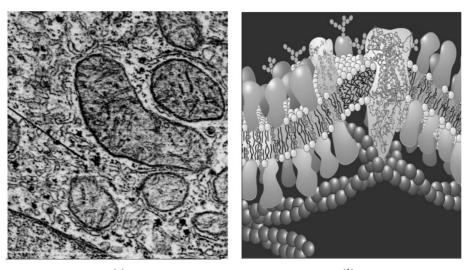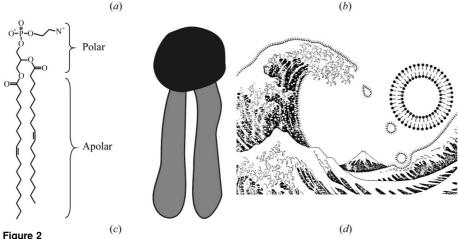
has an enormous affinity for itself. Another interesting property of lipidic materials is the fact that they can access the so-called 'fourth state of matter', the liquid-crystalline state (Fig. 3). Most materials will pass from a solid to a liquid state in response to a change in temperature, pressure and/or composition. In contrast, lipidic materials pass through one or several intermediate or liquid-crystalline phases (mesophases) during the solid-to-liquid transition. Liquid crystals have order intermediate between the crystalline solid and the isotropic liquid. Some of the liquid-crystalline phases that are accessed by lipids are shown in Fig. 3. For reference, schematics of the solid state and the liquid state are also included. The liquid-crystalline phases include the lamellar liquid-crystalline or L_α phase, cubic phases, hexagonal phases and others. The L_α phase has long been used as a successful model for the biological membrane.

1.2. Dynamic membrane processes

One of our research interests concerns the ubiquitous physiological process of membrane fusion. Much inter- and intracellular communication relies on the process. Fusion requires that two membranes come together to form a single continuous entity and that the contents of each membrane-bounded object mix in a non-leaky manner. This process involves structural rearrangements at the level of both the protein and the lipid components of the membrane. It has been proposed that fusion intermediates are reminiscent of the so-called non-lamellar phases introduced above. We investigate the dynamics and mechanism of the fusion process in simple systems and model it as a phase transformation of the lamellar-to-hexagonal or lamellar-to-cubic phase type. Such phase changes occur on a time-scale ranging from hours to milliseconds (Caffrey, 1989). The dynamics and mechanism of the transitions are studied using low- and wide-angle X-ray diffraction in the time-resolved mode. From a practical point of view, such measurements can only be made using a synchrotron source.

2. Radiation damage: background

Fig. 4 shows an example of the type of problem that we encounter with radiation damage as applied to lipidic systems. Where the beam strikes a dipalmitoylphosphatidylcholine (DPPC) or dimyristoylphosphatidylcholine (DMPC) sample, a footprint remains. The footprint probably appears as a result of chemical damage (see below), the products of which alter the dispersion state of the lipid and thus the way in which it scatters light (Caffrey, 1984). The footprints are long-lived, remaining in place for years. Note that other lipids such as dipalmitoleoylphosphatidylethanolamine (DiPOPE) and monoolein (MO) show no evidence of footprints after similar exposures.
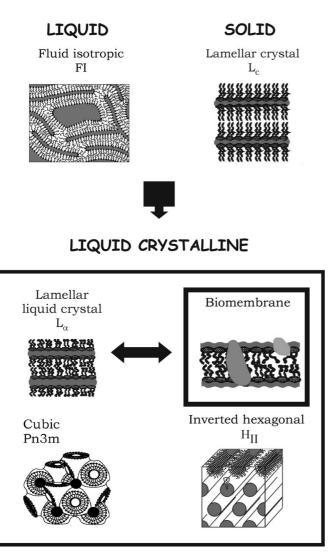
Fig. 5(a) shows a diffraction pattern obtained with a typical lipidic dispersion. It is a powder pattern consisting of a series of concentric rings in the low- and wide-angle regions. Most of the changes seen as a result of radiation damage occur in the low-angle region and correspond to changes in the long-range order of the sample. Scatter/diffraction at wide angles is attributed to lipid-chain packing and appears less sensitive to radiation damage. Thus far, our focus has been on the low-angle region.
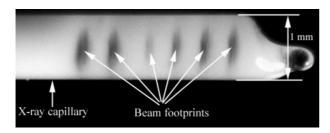
2.1. Damage: type I

We have observed two types of radiation damage with lipidic mesophases. Type I damage is illustrated in Fig. 5(b) and was observed using fully hydrated phosphatidylcholine (PC) in the lamellar gel ($L_{\beta'}$) phase. With time and accumulated dose, the higher-order lamellar reflections broaden and lose intensity while diffuse scatter develops, most noticeably in the region between the first- (d_{001}) and second-order (d_{002}) lamellar bands. 'Before' and 'after' diffraction patterns are shown in Fig. 5(c), where orientation in the diffuse scatter is apparent. This feature may be exploited in phasing the patterns, as described recently (Cherezov et al., 2000). Protein crystals undergoing radiation damage may yield similar phasing information, as reported in this issue (Ravelli et al., 2002).

Our initial attempts to quantify radiation damage of type I used a normalized order index (NOI; Cheng & Caffrey, 1996). The index is sensitive to the loss of diffraction

Figure 2
The nature of biological membranes: (a) electron micrograph of a rat liver cell in thin section; (b) model of biomembrane leaflet including lipids, integral and peripheral proteins, and cytoskeletal structures; (c) a representative glycerophospholipid, dioleoylphosphatidylethanolamine, with a cartoon to depict its amphipathic nature; (d) the self-assembling property of lipids as depicted in a modification of Hokusai's famous woodprint, origin unknown.

and its magnitude drops as diffuse scattering grows with accumulated dose and damage. An example is shown in Fig. 6(a) for the lamellar gel $L_{\beta'}$ and L_α phases of PC under conditions of full hydration. However, when the sample was exposed under conditions of water stress the NOI did not change appreciably, regardless of phase
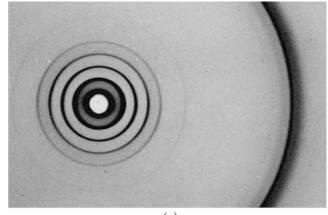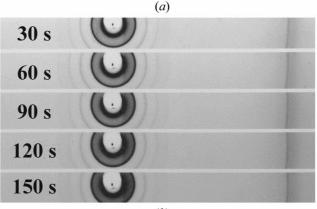

Figure 3
Common liquid, solid and liquid-crystalline phases formed by lipid assemblies.

Figure 4
Footprints due to beam damage in a fully hydrated lipid sample housed in a 1 mm-diameter quartz capillary. The sample was photographed using front illumination with a dark background. Damaged areas (footprints) are translucent and appear as dark spots in the photograph. This experiment was performed in May 2000 at the ESRF on beamline ID2 [12.5 keV, 6.3×10^{11} photons s^{-1}, 30 Mrad dose (for largest footprints) at 640 krad s^{-1}]. The sample was DPPC at 50% w/w water and 298 K.
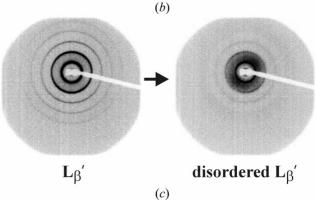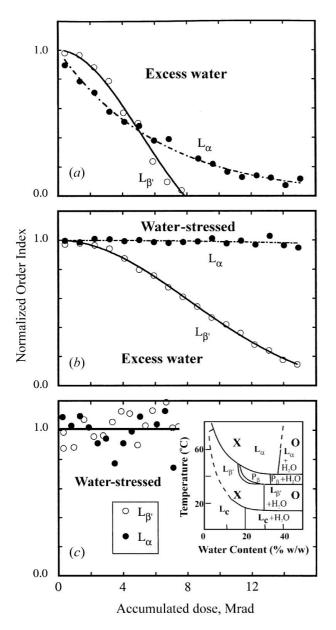

Figure 5
(a) Typical powder diffraction pattern for hydrated DPPC in the $L_{\beta'}$ phase recorded at 75% w/w water and 295 K (CHESS, A1 station, 6.3 mA, 5.2 GeV, 10 min exposure). (b) X-ray-induced changes in the mesophase structure of fully hydrated DPPC. Low- and wide-angle diffraction from the lipid recorded on X-ray-sensitive film is shown as a series of consecutive X-ray photographs (exposure time 30 s) recorded during continuous X-irradiation of the sample. Measurements were performed at 298 K in the $L_{\beta'}$ phase using focused monochromatic X-rays at 1.56 Å (8 keV) on the A1 station at CHESS. The incident flux on the sample was 1.7×10^{10} photons s^{-1} (18 krad s^{-1}). Each frame corresponds to a dose of 0.54 Mrad such that 150 s represents a total accumulated dose of 2.7 Mrad. The sample-to-detector distance was 11 cm, and sequential patterns were recorded in 1.0 cm-wide strips on a 12.5×17.5 cm Kodak DEF-5 X-ray-sensitive film. Elapsed times are indicated. (c) Changes in the low-angle diffraction pattern of the $L_{\beta'}$ phase of hydrated DPPC (50% w/w water) at 298 K induced by X-irradiation. After irradiation, diffuse scattering appears in the diffraction patterns, most prominently between the (001) and (002) reflections. Diffraction peaks and diffuse scattering are oriented in the 1 o'clock to 7 o'clock direction before and after exposure. Images before (left) and after (right) irradiation are shown. Experimental conditions include ESRF beamline ID2, 12.5 keV, 6.3×10^{11} photons s^{-1}, 490 krad s^{-1}, total accumulated dose of 59 Mrad. (b) is modified from Fig. 3 of Cheng & Caffrey (1996) and (c) is modified from Fig. 1 of Cherezov et al. (2000).

(Figs. 6*b* and 6*c*). If the NOI is an accurate measure of radiation damage, these results would indicate that the sample has not suffered damage at less than full hydration. The data shown in Fig. 7, however, prove unequivocally that damage does occur under conditions of water stress, but it is masked under these conditions.

This is a very important result because it means that *X-ray diffraction is not always a reliable indicator of radiation damage*.

The NOI proved to be a useful measure of the progress of radiation damage when it effected a change in the diffraction pattern. However, we have since separately quantified the development of
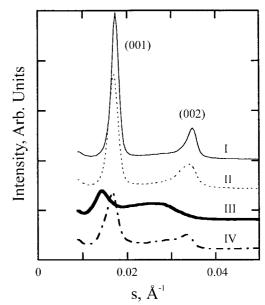

Figure 6
The effect of the hydration level on X-ray-induced changes in low-angle diffraction behavior of the (001) reflection of L_α (338 K) and the (001) reflection of $L_{\beta'}$ (303 K) phases of DPPC. (*a*) 46% *w/w* water; (*b*) 34% *w/w* water; (*c*) 14% *w/w* water. Lines are drawn to guide the eye. A schematic temperature-composition phase diagram for DPPC/water is shown as an inset in (*c*). In the inset, **X** and **O** identify, respectively, sample compositions where the water-stressed and fully hydrated conditions prevail. Diffraction patterns were collected on the A1 station at CHESS (8 keV, 2×10^{10} photons s^{-1}). Modified from Fig. 4 of Cheng & Caffrey (1996).

diffraction intensity and diffuse scatter as a measure of damage-induced stacking disorder within the lamellar phase (Cherezov *et al.*, 2000). Our long-term objective is to fit the entire diffraction curve taking into account stacking disorder and using a parameterized density of the lipid bilayer. This will allow us to obtain direct information on the growth of stacking disorder and on changes in lipid bilayer structure with accumulated dose.

2.2. Damage: type II

Type II damage is characterized by a partial or complete phase transformation that, unlike type I damage, is not accompanied by a change in phase order/disorder (Cheng *et al.*, 1993). Two examples of type II damage are shown in Figs. 8(*a*) and 8(*b*). These include the lamellar-to-inverted hexagonal (H_{II}) and the cubic *Pn3m*-to-H_{II} phase transitions. In both cases, we see a partial or complete change in phase but no line broadening or development of diffuse scatter. Typically, a certain accumulated or threshold dose is necessary to trigger the transition. Below that threshold, no changes in the diffraction pattern are seen. The threshold dose depends on how close in temperature the sample is to the corresponding transition (Cherezov *et al.*, 2000). The linear dependence of the threshold dose on the temperature differential indicates that the threshold drops to zero at precisely the transition temperature. This means that the

Figure 7
A test of the hypothesis that X-radiation damage, as monitored by X-ray diffraction, requires the presence of an excess-water phase for expression. Low-angle patterns from DMPC in the L_α phase (reflections are indicated in figure) at 34% *w/w* water (representing the water-stressed condition) were recorded at 302 K with 0 Mrad (I) and 50 Mrad (II) of X-ray exposure. Very little change in the diffraction pattern is apparent under these conditions of water stress. The sample giving rise to pattern II was subsequently cooled to 283 K, where the $L_{\beta'}$ phase forms under normal conditions, and the diffraction pattern (III) was recorded by irradiating in the same spot used to collect data for pattern II. Pattern III is what is expected for the extensively radiation-damaged $L_{\beta'}$ phase in excess water. At 283 K and an overall sample composition of 34% *w/w* water, this sample is expected to be under conditions of excess water. The pattern shown in IV was recorded by translating the capillary by 0.6 mm in the direction perpendicular to the X-ray beam to expose a region of the sample that had not previously been X-irradiated. Pattern IV is typical of the $L_{\beta'}$ phase in equilibrium with excess water. Diffraction patterns were collected on the A1 station at CHESS (8 keV, 2×10^{10} photons s^{-1}). Modified from Fig. 7 of Cheng & Caffrey (1996).
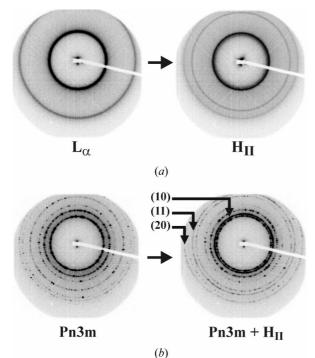
closer to the transition temperature the measurement is made, the smaller is the dose needed to effect noticeable damage of type II.

2.3. X-rays 'do chemistry'

In the set of experiments described in §2.1, the sample underwent radiation damage but this was not apparent in the diffraction pattern under water-stressed conditions. Accordingly, we set about identifying a more reliable indicator of radiation damage. It seemed likely that the changes induced as a result of damage had their origins in the chemical modification of the lipid, since X-rays are energetic particles with the capacity to ionize and to trigger reactions. We looked for evidence of X-ray-induced chemical change using thin-layer chromatography. The data in Fig. 9 show clearly that X-irradiation is accompanied by chemical decomposition, which occurs regardless of the state of hydration of the sample. This is consistent with the results noted in §2.1. In addition to chemical breakdown leading to the production of fatty acids and lyso-lipids (Caffrey, 1984; Cheng et al., 1993), it is likely that lipidic polymers are produced as a consequence of damage. Evidence in support of this comes from the streaking observed close to the origin in the thin-layer chromatogram (Fig. 9, lanes 3 and 4). Our intent is to use mass spectrometry to characterize more fully these and other damage products.

2.4. Beam heating

The transitions described in §2.2 were observed when the sample was held at a temperature below the corresponding phase-transition temperature. It was suggested, therefore, that the effect seen might simply be due to beam heating. Clearly this is not the case, as the new phase formed as a result of X-irradiation persists after the beam is turned off and the sample is allowed to thermally re-equilibrate. Of course, this assumes that the high-temperature phase does not undercool. Nonetheless, we were interested in quantifying the heating capability of the X-ray beam and an experiment was set up to make the measurement illustrated in Fig. 10. This used a very small thermocouple positioned in the sample capillary to one side of the X-ray beam. A miniscule rise in temperature, amounting to 0.16 K, was recorded from an initial temperature of 288.35 K. The measurement is compromised to some degree by the fact that the thermocouple itself can act as a thermal conduit. Nevertheless, the magnitude of the temperature change is so small that it is unlikely to contribute in a significant way to the type II damage noted above. Future investigations of beam heating will use non-invasive thermal imaging as described in this issue (Snell et al., 2002).

2.5. Damage 'in the dark'

It seems reasonable to expect that damage takes place while the sample is being irradiated, and, indeed, this is what is observed, as described above. Less intuitive is the possibility of witnessing damage 'in the dark' following an exposure, when the X-ray beam is turned
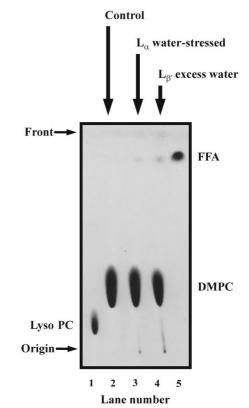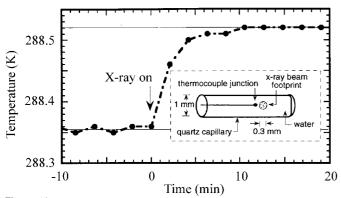

Figure 8
Changes in low-angle diffraction induced by type II X-ray damage. Images before (left) and after (right) irradiation. (a) Methylated dioleoylphosphatidylethanolamine (DOPE-Me), 70% w/w water, 328 K, 12.5 keV, 473 krad s^{-1}, 6.3×10^{11} photons s^{-1} and a total accumulated dose of 283 Mrad, where the L_α phase transforms to the H_{II} phase. (b) MO, 40% w/w water, 354 K, 12.5 keV, 375 krad s^{-1}, 6.3×10^{11} photons s^{-1} and a total accumulated dose of 228 Mrad, where the cubic Pn3m phase transforms partially to the H_{II} phase. The first three H_{II} reflections are indicated. Patterns were generated on the ID2 beamline at the ESRF. Modified from Fig. 1 of Cherezov et al. (2000).

Figure 9
Thin-layer chromatogram of X-irradiated (lanes 3 and 4) and control (non-irradiated, lane 2) samples of DMPC at 34% w/w water to reveal chemical changes induced by continuous exposure to X-rays. The irradiated sample had been in the uncollimated 13.6 keV X-ray beam on the F1 station at CHESS (2×10^{11} photons s^{-1}) for 5.6 min (~50 Mrad) at 302 K (in the water-stressed L_α phase, lane 3) or 283 K (in the fully hydrated $L_{\beta'}$ phase, lane 4). Both samples show significant chemical breakdown. The extent of the radiation damage as monitored by X-ray diffraction was recorded after the exposure. The solvent system was chloroform:methanol:water (65:25:4 by vol.). The lipid standards used were 1-palmitoyl-sn-glycero-3-phosphocholine (lyso PC), lane 1, and palmitic acid (FFA), lane 5. Modified from Fig. 6 of Cheng & Caffrey (1996).

off. However, we have seen this phenomenon and it shows up in two distinct forms. In the first, radiation damage is already under way and is evident before the beam is turned off. After some delay in the dark, the sample is re-examined. Such an example is shown in Fig. 11(a), where clearly damage continues in the absence of X-irradiation. In the second form, the initial dose is low enough to cause no apparent damage (Fig. 11b). However, turning off the beam and waiting for an interval before re-examining the sample shows that damage had already set in during the initial exposure and that the process that gave rise to a change in the diffraction pattern had continued in the dark. It may be that the primary damage products are generated immediately during the exposure and that secondary products, plus the attendant phase change, happen subsequently and more slowly.

This is an important result with consequences for how samples are handled during synchrotron-based measurements. Thus, for example, the sample may be exposed to the X-ray beam transiently during capillary alignment, and the diffraction pattern may show no evidence of radiation damage after such brief exposures. The actual subsequent measurement is likely to involve a change in one or several conditions. The observed phase behavior could, therefore, be compromised by the products of a reaction that took place 'in the dark' while preparations were being made for data collection. This problem could be overcome by aligning on one part of the sample and making measurements on an adjacent, previously unexposed, part of the sample. This is routine in electron diffraction and microscopic measurements.

2.6. A free-radical-mediated process

Ionizing radiation, such as X-rays, interacts with biomaterials in ways that are expected to produce free radicals. We suspected that the damage described above was free-radical mediated. The problem with detecting free radicals is that they are usually short-lived and thus difficult to monitor. Electron spin resonance (ESR) is commonly used for measuring free radicals. However, unless the ESR measurement is made while the sample is being irradiated it is
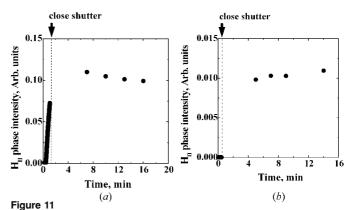
unlikely that the signal will persist and be measurable in a post-irradiation assay. Spin traps can be used to advantage here, since they react with the transient radical and produce a long-lived species that can be measured at a later time. This approach was taken in the current study, and the results of a spin-trap (2-methyl-2-nitrosopropane) measurement are shown in Fig. 12. Clearly, free-radical generation in the presence of the lipid is over and above that seen when the dispersing medium alone is subjected to X-irradiation. This study demonstrates convincingly that free radicals are produced when the hydrated lipid is exposed to X-rays. It is very likely that these reactive species go on to trigger chemical transformations that give rise to what we detect by chromatography and diffraction as radiation damage.

2.7. Dispersing-medium effects

Since the cryo-cooling approach is not really an option in studies of lipid mesophase behavior, we would like to explore the possibility of

Figure 11
Evidence that beam damage continues when the sample is no longer being exposed to X-rays. Appearance of the H_{II} phase (10) reflection in an L_α-phase background after exposing hydrated DiPOPE to (a) an accumulated dose of 46 Mrad or (b) a sub-threshold dose of 16 Mrad, before closing the shutter for 5 min then reopening to collect diffraction data. Data were collected on the ID2 beamline at the ESRF (12.5 keV, 6.3×10^{11} photons s^{-1}, 640 krad s^{-1}). Measurements were made with samples at 50% w/w buffer (150 mM NaCl, 20 mM TES, pH 7.4) and 305.5 K. Sample preparation is similar to the protocol described by Cherezov et al. (2000).

Figure 10
Heating effect of a 13.6 keV X-ray beam with a flux of 2×10^{10} photons s^{-1}. The temperature rise was recorded using a T-type thermocouple junction (0.005 inch OD thermocouples; Omega Technologies Company, Stamford, CT, USA) positioned in a 1 mm quartz capillary filled with Milli-Q water. The capillary was adjusted initially to position the junction directly in the X-ray beam. The capillary and thermocouple were then translated by 0.3 mm perpendicular to the X-ray beam along the length of the capillary so that the thermocouple was just to one side and within 0.3 mm of the X-ray beam (see inset). The temperature rise was recorded upon opening the beam shutter. Positioning of the thermocouple junction in the X-ray beam was facilitated by using a real-time X-ray area detector to monitor directly the shadow cast by the junction on diffuse X-ray scattering. This study was performed on the A1 station at CHESS. Taken from Fig. 11 of Cheng & Caffrey (1996).
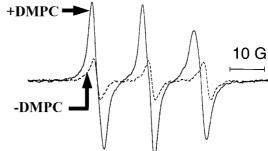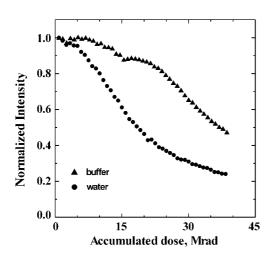

Figure 12
ESR spectrum of an aqueous spin-trap solution after X-irradiation in the presence (+) and absence (−) of DMPC. Hyperfine-splitting constants are 15.2 G and 16.0 G, respectively. The total dose in each case was 15 Mrad (61% absorption assumed) and exposures were made at a dose rate of 14 krad s^{-1}. Radicals observed are stable for at least a week at 277 K. The ESR spectra were obtained at room temperature with the following ESR spectrometer settings: microwave power, 20 mW; field, 3465 ± 50 G; conversion, 163.84 ms; time constant, 655 ms; sweep time, 167.772 s; modulation frequency, 100.000 kHz; modulation amplitude, 1.013 G; receiver gain, 5×10^5; number of scans, 1. Samples were irradiated with a flux of 2×10^{10} photons s^{-1} on the A1 beamline at CHESS. Taken from Fig. 2 of Cheng & Caffrey (1996).

adding free-radical scavengers and deoxygenation as strategies for minimizing radiation damage. These manipulations will be of use only if they do not impact on the phase properties of the system. A limited number of such studies have been performed (Cheng & Caffrey, 1996). One example is shown in Fig. 13, where the X-ray sensitivity of the gel phase ($L_{\beta'}$) in hydrated DPPC was evaluated in the presence of a TES/NaCl buffer system at pH 7.4. TES (*N*-tris[hydroxymethyl]methylaminoethane sulfonic acid) has been reported to act as a free-radical scavenger (Fiorentini *et al.*, 1989). As judged by the changing diffraction pattern, damage was significantly reduced in the presence of the buffer system. We are currently investigating the origin of this effect. It is possible that the buffer is acting as a free-radical scavenger and in this way is minimizing damage. It is also possible that damage is taking place but the effect is being masked as a result of charge screening by the salt.

2.8. Dose-rate effects

The data above demonstrate that radiation damage is free-radical mediated. Thus, the progress of damage is expected to be time-dependent in that radicals and the damage products they create must migrate in the sample to allow for the expression of damage. Regardless of how fast the latter processes are, with a hot enough beam it should be possible to deliver enough photons to the sample to produce a measurable signal (the diffraction pattern) in a time shorter than it takes for damage to develop and to reveal itself. The higher flux density is also associated with a greater probability of free radicals combining with one another and thereby limiting damage. This is the so-called 'inverse dose-rate effect'. Specifically, damage should be less severe for a given accumulated dose as the number of incident photons per unit time and per unit area (dose-rate) rises.

In the course of this work, we have studied the dose-rate effect at several synchrotron facilities and under a variety of conditions. The first result is shown in Fig. 14(*a*), where radiation damage of type I was examined at beamline ID2 (ESRF) using fully hydrated DPPC in the $L_{\beta'}$ phase at 298 K. The loss of diffraction at low angles was monitored as a function of accumulated dose, calculated as described previously (Cherezov *et al.*, 2000), over the dose-rate range 2–640 krad s^{-1}. In this experiment, the dose was delivered continuously in the sense that the sample was irradiated without interruption as dose accumulated. Worthy of note in this regard is the timed structure of the source itself. The data show a distinct inverse dose-rate effect. Thus, for a given accumulated dose, the higher dose rate produced less damage.
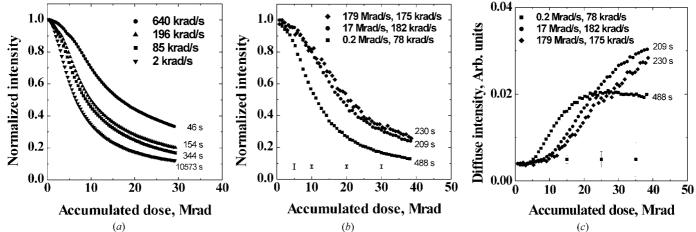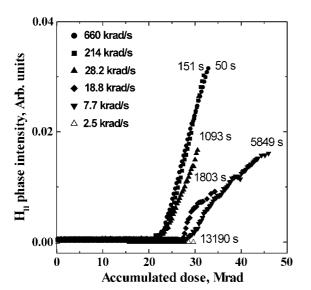

Figure 13
Type I damage to hydrated DPPC at 50% *w/w* water or buffer (150 m*M* NaCl, 20 m*M* TES, pH 7.4) and 298 K as a function of accumulated dose. Loss of $L_{\beta'}$ phase (001) reflection intensity with accumulated dose with a 10.0 keV beam operated at a flux of 5.4×10^{13} photons s^{-1} and discontinuous (pulsed) sample irradiation. $L_{\beta'}$ phase intensities at a particular accumulated dose were normalized against the intensity for zero accumulated dose. The dose rates were 17 Mrad s^{-1} within the pulse and 185 krad s^{-1} when averaged over the sum of the pulse time (50 ms) and the dead time (4.5 s). Data were collected at APS on beamline 18ID. Sample preparation is similar to the protocol described by Cherezov *et al.* (2000).

Figure 14
Type I damage to hydrated DPPC at 50% *w/w* water and 298 K as a function of accumulated dose and dose rate. (*a*) Loss of $L_{\beta'}$ phase (001) reflection intensity with accumulated dose with a 12.5 keV beam operated at a maximum flux of 6.3×10^{11} photons s^{-1} (attenuation achieved with metal foils) and continuous sample irradiation. The dose rates are indicated in the panel. Measurements were performed at the ESRF on beamline ID2. (*b*) Loss of $L_{\beta'}$ phase (001) reflection intensity with accumulated dose at 10.0 keV, 5.4×10^{13} photons s^{-1} and discontinuous (pulsed) sample irradiation. (*c*) Increase in diffuse scattering intensity between the (001) and (002) low-angle reflections of the $L_{\beta'}$ phase with accumulated dose. Typical standard deviations calculated based on triplicate samples are indicated below the curves in (*b*) and (*c*) for samples irradiated at 179 Mrad s^{-1} and 17 Mrad s^{-1}. Elapsed time (in s) at the end of each exposure is indicated. $L_{\beta'}$ phase intensities presented in (*a*) and (*b*) were normalized as described in the legend to Fig. 13. The dose rates indicated in (*b*) and (*c*) were calculated for the period of irradiation and for the sum of the period of irradiation (5 ms to 5 s) and the dead time (4.5 s). Data shown in (*b*) and (*c*) were collected at the APS on beamline 18ID. Sample preparation is similar to the protocol described by Cherezov *et al.* (2000).

A similar result was obtained at beamline 18ID (APS) under conditions of *discontinuous* irradiation (Fig. 14*b*). The latter course of photon delivery was necessitated by the dead time of the detector (CCD, 4.5 s) during image readout and data transfer. Thus, the damage protocol involved a series of sequential fixed-interval exposures and data collection followed by a period of 4.5 s where the beam was turned off and the image was read out. The maximum dose rate available under these conditions (179 Mrad s^{-1}) was more than two orders of magnitude higher than at any other source we had used. However, in contrast to previous studies, damage was generated with discontinuous as opposed to continuous irradiation. Attenuation was achieved using metal foils, and the duration of each exposure interval was adjusted to the same accumulated dose for all dose rates studied. The results in Figs. 14(*b*) and 14(*c*) show that the same inverse dose-rate effect was observed as that noted above with continuous irradiation at the lower overall dose-rate levels.

Thus, type I damage demonstrates the inverse dose-rate effect regardless of whether the exposure is continuous or discontinuous. In distinct contrast, type II damage to DiPOPE suggests the opposite effect under conditions of continuous exposure (Fig. 15). It must be appreciated that this experiment has not been repeated many times. Nevertheless, the threshold would appear to lengthen and the rate of damage with accumulated dose drops slightly at the lower dose rates.
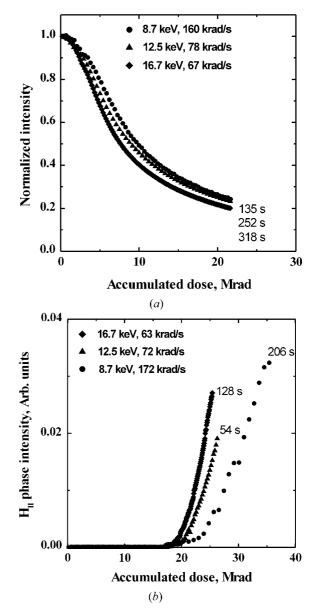
To what can we attribute the opposite dose-rate effects seen with type I and type II damage? One possibility is that the inverse dose-rate effect applies to both, but the systems and the conditions are so different as to give rise to these disparate results. To begin with, type I measurements were made in the $L_{\beta'}$ phase, where the lipid molecules have very limited mobility. Conversely, type II damage occurred in the L_α phase, where rapid diffusion in the plane of the membrane is a characteristic of the phase. Thus, under type I conditions, damage products are more likely to accumulate where generated and to elicit the damage effect *in situ*. This is in contrast to the more fluid L_α

phase, where products may diffuse away from the site of production, allowing the effect to lessen with time as a result of simple dilution. Thus, at the higher dose rates, damage products will be more concentrated because they will have had less time to diffuse away for a given accumulated dose. Another factor to consider is the heating effect of the beam. The temperature along the track of the beam in the sample will be higher at the higher dose rate [see calculations in Cheng & Caffrey (1996) and Kuzay *et al.* (2001)]. Thus, type II damage, which happens when close to a phase transition (see above), should occur sooner at the higher dose rate. The higher associated heating effect simply shifts the system closer to the phase-transition

(a)

(b)

Figure 15
Effect of dose rate on type II damage in hydrated DiPOPE at 50% *w/w* buffer (150 m*M* NaCl, 20 m*M* TES, pH 7.4) and 305.5 K. The H_{II} phase intensity on the ordinate axis corresponds to the integrated diffraction signal in the (10) reflection of the H_{II} phase that appears on a background of the L_α phase. The dose rate and the elapsed time (in s) at the end of each exposure are indicated. Measurements were made at the ESRF on beamline ID2 (12.5 keV, maximum flux 6.3 × 10^{11} photons s^{-1}, attenuation achieved by using metal foils) under conditions of continuous sample irradiation. Sample preparation is similar to the protocol described by Cherezov *et al.* (2000).

Figure 16
Effect of beam energy on (*a*) type I damage in hydrated DPPC (50% *w/w* water, 298 K) and (*b*) type II damage in hydrated DiPOPE [50% *w/w* buffer (150 m*M* NaCl, 20 m*M* TES, pH 7.4) at 305.5 K]. The dose rates at each beam energy are indicated in the panels, as is the elapsed time after the last exposure (in s, beside each data series). The incident fluxes were 6.2 × 10^{10} photons s^{-1} for 8.7 keV, 6.3 × 10^{10} photons s^{-1} for 12.5 keV and 9.1 × 10^{10} photons s^{-1} for 16.7 keV. Experiments were performed using beamline ID2 at the ESRF under conditions of continuous irradiation. Sample preparation is similar to the protocol described by Cherezov *et al.* (2000).

temperature. As noted under type II damage, a smaller temperature differential corresponds to a smaller accumulated dose threshold. This may partly explain what is happening in Fig. 15.

The foregoing argument assumes that the incident beam has a uniform profile [number of photons /(unit time, unit area)] and thus is free of 'hot spots'. The complicating issue of hot spots in the context of radiation damage has been addressed by Cheng & Caffrey (1996). Measurements reported in this paper that were made at the ESRF and the APS also involved beam profiling. In both cases, a Gaussian distribution was observed (in the horizontal and vertical directions).

2.9. Photon energy

One of the benefits of using a synchrotron beam is that it can be tuned over a relatively wide energy range. Each source has a characteristic output spectrum, and monochromators are commonly used to isolate particular wavelengths. Since damage due to ionizing radiation depends to some degree on photon energy, we evaluated beam damage as a function of energy in the range 9–17 keV. Measurements were made at beamline ID2 (ESRF) by monitoring the progress of type I and II damage, respectively, in hydrated DPPC and DiPoPE as above. It is important to note that many properties of the system change and must be corrected and/or accounted for as photon energy is changed. These include, but are not limited to, beam size, dose rate, beam profile, beam heating, transmission (through air, windows, sample container, the sample itself), scattering/diffraction properties, and beam-intensity monitor (ion chamber, photodiode) and detector sensitivity. Although every effort was made to control these effects, we found that the dose-rate differed by a factor of two at the low and high energies used. The results of the study are included in Fig. 16. The data suggest that there is no large energy effect on damage in the range studied. The differences seen as a function of photon energy are similar to those due to sample variability, which can be pronounced at high accumulated doses (Fig. 14c). Note that while the latter stages of type II damage seen in Fig. 16(b) are somewhat slower to develop with accumulated dose at the lower energy, the threshold for onset of damage is insensitive to photon energy at all three energies.

Given that an energy effect was not observed in this study, our recommendation is to choose that energy which optimally combines source output, scatter/diffraction efficiency and detector sensitivity.

3. Concluding remarks

The results presented above demonstrate that studying soft condensed biomaterials, such as lipids and membranes, with a bright X-ray source such as that available at a synchrotron can lead to problems with radiation damage. Provision must be made in all such studies to look for the effect and to take measures to ensure that data collection is not compromised by damage.

Because radiation damage was recognized only very recently as an issue worthy of study, little focused research has been carried out in the area. As a result, few useful rules or principles have emerged as to the types of materials that are more or less prone to radiation damage. Likewise, sample dispersion conditions and beam characteristics that minimize damage have not been fully investigated. Currently, therefore, each sample type must be evaluated on an individual basis. We need general guidelines, and beam time must be allocated for the purpose of establishing them. Our studies of photon energy showed little difference in radiation damage in the 9–17 keV range. Both direct and inverse dose-rate effects were observed with the different damage types examined.

While the rules and principles governing radiation damage in this area have not yet been identified, we can state with confidence that X-ray diffraction is not a reliable indicator of radiation damage. Thus, under the right conditions, radiation damage can exist and go unnoticed. The problem is that it can express itself when conditions change, thereby rendering useless the entire measurement or study.

We make extensive use of synchrotron radiation despite the problem of radiation damage, and we do so without resorting to beam attenuation. Fortunately, we work with long homogenous samples held in glass capillaries. Thus, the sample is continuously moved in the beam during a measurement to ensure that no one part is over-exposed. It is important to realize that cryo-techniques are not an option in this area of membrane/lipid research, where measurements are typically made in the temperature range 273–323 K.

Over the past two decades we have worked at the APS, CHESS, ESRF and NSLS. We have had to deal with the problem of radiation damage at all but the latter. The beam at NSLS is divergent/convergent. Further, we focus the beam at the detector, which means that the swath of radiation striking the sample is relatively large, and thus the X-ray flux density at the sample is relatively low. This spares the sample from noticeable damage.

We have demonstrated that free radicals are produced as a result of X-irradiation. These reactive species have the capacity to 'do chemistry', resulting in changes in molecular structure and, by extension, mesophase identity and microstructure. Type II damage involves a phase transformation, which can be of the lamellar-to-non-lamellar form. In this context, it is interesting to note that biomembranes are usually of a lipid constitution, such that they exist under physiological conditions close to such a transition and are particularly sensitive to type II damage. Should a lamellar-to-non-lamellar transition take place in the lipid component of the biomembrane, its integrity would be compromised, producing a leaky structure incapable of supporting a gradient. This unhealthy state would probably lead to cell death if left unrepaired. Free-radical production is associated with aging and other physiological and non-natural processes. Excessive accumulations of free radicals could trigger a local phase transformation of the type described, leading to a loss of selective permeability and the ability to support gradients and, ultimately, to cell death. It is interesting that these insights into important physiological issues were arrived at as a spin-off from a study of the nagging problem of radiation damage.

References

Caffrey, M. (1984). *Nucl. Instrum. Methods Phys. Res.* **222**, 329–338.
Caffrey, M. (1989). *Annu. Rev. Biophys. Biophys. Chem.* **18**, 159–186.
Cheng, A. & Caffrey, M. (1996). *Biophys. J.* **70**, 2212–2222.
Cheng, A., Hogan, J. L. & Caffrey, M. (1993). *J. Mol. Biol.* **229**, 291–294.
Cherezov, V., Cheng, A., Petit, J.-M., Diat, O. & Caffrey, M. (2000). *Cell. Mol. Biol.* **46**, 1133–1145; erratum (2001). **47**, 229–230.
Fiorentini, D., Landi, L., Barzanti, V. & Cabrini, L. (1989). *Free Radical Res. Commun.* **6**, 243–250.
Kuzay, T. M., Kazmierczak, M. & Hsieh, B. J. (2001). *Acta Cryst.* D**57**, 69–81.
Ravelli, R. B. G., Theveneau, P., McSweeney, S. & Caffrey, M. (2002). *J. Synchrotron Rad.* **9**, 355–360.
Snell, E. H., Judge, R. A., Larson, M. & van der Woerd, M. J. (2002). *J. Synchrotron Rad.* **9**, 361–367.